Detection and Tracking of Multipath Channel Parameters Using Belief Propagation

Li, Xuhong; Leitinger, Erik; Tufvesson, Fredrik

Published in:
IEEE Asilomar Conference on Signals, Systems, and Computers

DOI:
10.1109/IEEECONF51394.2020.9443465

2021

Document Version:
Peer reviewed version (aka post-print)

Detection and Tracking of Multipath Channel Parameters Using Belief Propagation

Xuhong Li*, Erik Leitinger†, and Fredrik Tufvesson*
*Department of Electrical and Information Technology, Lund University, Sweden.
†Signal Processing and Speech Communication Laboratory, Graz University of Technology, Austria
Email: {xuhong.li, fredrik.tufvesson}@eit.lth.se, erik.leitinger@tugraz.at

***Abstract*—We present a belief propagation (BP) algorithm with probabilistic data association (DA) for detection and tracking of specular multipath components (MPCs). In real dynamic measurement scenarios, the number of MPCs reflected from visible geometric features, the MPC dispersion parameters, and the number of false alarm contributions are unknown and time-varying. We develop a Bayesian model for specular MPC detection and joint estimation problem, and represent it by a factor graph which enables the use of BP for efficient computation of the marginal posterior distributions. A parametric channel estimator is exploited to estimate at each time step a set of MPC parameters, which are further used as noisy measurements by the BP-based algorithm. The algorithm performs probabilistic DA, and joint estimation of the time-varying MPC parameters and mean false alarm rate. Preliminary results using synthetic channel measurements demonstrate the excellent performance of the proposed algorithm in a realistic and very challenging scenario. Furthermore, it is demonstrated that the algorithm is able to cope with a high number of false alarms originating from the prior estimation stage.**

I. Introduction

The information of dispersive wireless radio channels in delay, angular, and frequency domain, and its temporal behavior in dynamic scenarios are of great importance for the design and development of radio-channel models [1], [2], 5G wireless communication technologies [3]–[5], and multipath-based localization and mapping [6]–[8]. The response of a wireless radio channel is typically represented by superimposed multipath components (MPCs) with parameters such as delay, angle-of-arrival (AoA), and angle-of-departure (AoD). These MPC parameters are usually estimated from multidimensional radio measurements using antenna arrays and multiple frequencies (wide-band or ultrawide-band signals) using super-resolution parametric channel tracking algorithms that perform sequential estimation of specular MPCs (SMCs).

A. State of the Art Methods

The existing MPC tracking algorithms can be grouped into two broad categories. Algorithms of the first category estimate and track the MPC parameters directly based on the radio signals using for example an extended Kalman filter (EKF) [9], [10]. Algorithms of the second category are based on a two-stage approach, where a snapshot-based parametric channel estimator such as [11]–[13] is incorporated into a tracking filter [14], or extended with a state-transition model that enables sequential Bayesian estimation [15]. In this work, we focus on the two-stage algorithms. In general, the correct model order (number of SMCs) is unknown, time-varying and need to be estimated, i.e., the model-order selection problem. One classical solution is to extend the tracking algorithm with an outer stage for model order detection using for example eigenvalue-based methods, or the generic information theoretic criteria, e.g., the Akaike/Bayesian information criterion. Another choice is to adopt sparsity-based algorithms, which aim to reconstruct sparse signals from a reduced set of measurements specified by a sparse weight vector. By introducing a sparsity-promoting prior model for the weights, the estimation of model order and MPC parameters can be jointly formulated inside a Bayesian framework. Most of the sparsity-based algorithms [16]–[18] are proposed for time-invariant measurement. Examples of sparsity-based sequential Bayesian algorithms are given in [15], [19]. In addition to the model-order selection, data association (DA) i.e., which measurement originates from which MPC, is potentially another problem for two-stage methods. In general, existing methods adopt single hypothesis, i.e., the state of each MPC is updated using a single measurement specified by the metrics such as the global nearest neighbor [20]. In comparison, probabilistic DA [20], [21] which evaluates all the current measurements for the update of each predicated MPC state would be more preferable in the presence of false alarm measurements.

B. Contributions

In this work, we propose a belief propagation (BP) -based algorithm for MPC detection and tracking (abbreviated as BP-MPCT) which uses the MPC estimates from a parametric super-resolution sparse Bayesian variational (abbreviated as SBL) channel estimator as measurements. This BP-MPCT algorithm jointly performs probabilistic DA and sequential estimation of potential specular MPC (PSMC) parameters and mean number of false alarms. Probabilistic DA and state estimation are performed by running BP on a factor graph [8], [21]. We use a probabilistic model for MPC existence where each PSMC state is augmented by a binary existence variable and associated with a probability of existence, which is also estimated and used for detection of the reliable MPCs modeling the birth and death. Inspired by [22]–[24], the algorithm also exploits the estimates of mean and variance of the complex amplitudes to calculate the detection probabilities of path components. It is therefore also suitable for unknown and time-varying detection probabilities [25].

II. Problem Formulation

A. Radio Signal Model

We consider a single-input–multiple-output (SIMO) channel model, where a baseband radio signal $s(t)$ is transmitted from a mobile user (UE) to a base station (BS) equipped with an antenna array of J elements. For the sake of simplicity we assume a two dimensional scenario with horizontal-only propagation.[1] The received signal at each antenna element indexed by $j \in \{1, \ldots, J\}$ is given as

$$r^{(j)}(t) = \sum_{l=1}^{L_t} \alpha_{l,t} s\big(t - f(\tau_{l,t}, \varphi_{l,t}, \boldsymbol{p}^{(j)})\big) + w(t), \quad (1)$$

where the first term comprises L_t SMCs, with each being characterized by the complex amplitude $\alpha_{l,t}$, the time delay $\tau_{l,t}$ to the array's center of gravity, and the AoA $\varphi_{l,t}$ with respect to the array orientation. The function $f(\tau_{l,t}, \varphi_{l,t}, \boldsymbol{p}^{(j)})$ maps the SMC parameters from the array's center to the position $\boldsymbol{p}^{(j)}$ of the jth array element [26]. We assume that the UE and BS are time synchronized and the array orientation is known. The second term $w(t)$ in (1) represents the measurement noise which is described by additive white Gaussian noise (AWGN) with double-sided power spectral density $N_0/2$.

The received signal $r^{(j)}(t)$ observed over a duration T is sampled with frequency $f_s = 1/T_s$, yielding a length $N_\mathrm{s} = T/T_\mathrm{s}$ sample vector $\boldsymbol{r}_n^{(j)} \in \mathbb{C}^{N_\mathrm{s}\times 1}$ from each array element, and n is the discrete time index. By stacking $\boldsymbol{r}_n^{(j)}$ from J array elements, the discrete time signal vector $\boldsymbol{r}_n \triangleq [(\boldsymbol{r}_n^{(1)})^\mathrm{T}, \ldots, (\boldsymbol{r}_n^{(J)})^\mathrm{T}]^\mathrm{T} \in \mathbb{C}^{N_\mathrm{s}J\times 1}$ is given as

$$\boldsymbol{r}_n = \boldsymbol{S}(\boldsymbol{\theta}_n)\boldsymbol{\alpha}_n + \boldsymbol{w}_n, \quad (2)$$

where $\boldsymbol{S}(\boldsymbol{\theta}_n) \triangleq [\boldsymbol{s}(\boldsymbol{\theta}_{1,n}), \ldots, \boldsymbol{s}(\boldsymbol{\theta}_{L_n,n})] \in \mathbb{C}^{N_\mathrm{s}J\times L_n}$ with $\boldsymbol{s}(\boldsymbol{\theta}_{l,n}) \in \mathbb{C}^{N_\mathrm{s}J\times 1}$ accounting for signal samples of the lth SMC from all array elements, and $\boldsymbol{\alpha}_n \triangleq [\alpha_{1,n}, \ldots, \alpha_{L_n,n}]^\mathrm{T} \in \mathbb{C}^{L_n\times 1}$. The SMC parameter vector is $\boldsymbol{\theta}_n \triangleq [\boldsymbol{\theta}_{1,n}^\mathrm{T}, \ldots, \boldsymbol{\theta}_{L_n,n}^\mathrm{T}]^\mathrm{T}$, with $\boldsymbol{\theta}_{l,n} \triangleq [\tau_{l,n}, \varphi_{l,n}]^\mathrm{T}$. The vector $\boldsymbol{w}_n$ contains the sampled AWGN from all array elements. A SMC exists only during the time duration (i.e., lifetime) that the BS/associated environment features are visible at the UE position. We assume that the true model order L_n is unknown and time-varying in dynamic measurement scenarios.

B. Parametric Channel Estimation

At each time n, a SBL channel estimator [12], [16]–[18] is used to estimate the SMC parameters $\hat{\boldsymbol{\theta}}_n \triangleq [\hat{\boldsymbol{\theta}}_{1,n}^\mathrm{T}, \ldots, \hat{\boldsymbol{\theta}}_{M_n,n}^\mathrm{T}]^\mathrm{T}$ with $\hat{\boldsymbol{\theta}}_{m,n} = [\hat{\tau}_{m,n}, \hat{\varphi}_{m,n}]^\mathrm{T}$, the mean value vector $\boldsymbol{\mu}_{\alpha,n} \triangleq [\mu_{\alpha,1,n}, \ldots, \mu_{\alpha,M_n,n}]^\mathrm{T}$ and covariance matrix $\boldsymbol{\Sigma}_{\alpha,n} \in \mathbb{C}^{M_n\times M_n}$ of corresponding complex amplitudes and the model order M_n. During the estimation process, we assume that miss detection of SMCs and estimation of MPCs which did not originate from any distinct environment features might occur. Hence, M_n is time-varying and it can be equal to, or larger/smaller than the true model order L_n. We also introduce the normalized amplitude $\hat{u}_{m,n} = \sqrt{\mathrm{SNR}_{m,n}}$ with $\mathrm{SNR}_{m,n} = |\mu_{\alpha,m,n}|^2/[\boldsymbol{\Sigma}_{\alpha,n}]_{m,m}$ as the square root of the estimated posterior signal-to-noise ratio (SNR) of the mth SMC [23], [24]. The normalized amplitudes $\hat{u}_{m,n}$ are directly related to the detection probabilities of the estimated SMCs as introduced in Sections III-C and III-D.

The estimates are stacked into the vector $\boldsymbol{z}_n \triangleq [\boldsymbol{z}_{1,n}^\mathrm{T}, \ldots, \boldsymbol{z}_{M_n,n}^\mathrm{T}]^\mathrm{T}$, where $\boldsymbol{z}_{m,n} \triangleq [\hat{d}_{m,n}, \hat{\varphi}_{m,n}, \hat{u}_{m,n}]^\mathrm{T}$ with $\hat{d}_{m,n} = c\hat{\tau}_{m,n}$ and c denotes the speed of light. We also define the vectors $\boldsymbol{z} \triangleq [\boldsymbol{z}_1^\mathrm{T}, \ldots, \boldsymbol{z}_n^\mathrm{T}]^\mathrm{T}$ and $\boldsymbol{m} \triangleq [M_1, \ldots, M_n]^\mathrm{T}$. The vector $\boldsymbol{z}$ is further used as noisy measurements in the BP-MPCT algorithm.

C. Inference Problem

Given all the past and current measurements $\boldsymbol{z}$, our goal is to infer the time-varying states of the SMCs, as well as the model order. Besides, the unknown and potentially time-varying false alarm measurement rate and detection probabilities are automatically adapted online, which avoids manually tunning of these measurement parameters for different datasets.

III. System model and Statistical Formulation

A. PSMC States and Dynamics

At each time n, the numbers of emerging SMCs and the SMCs that survived from the previous time are unknown. To account for this fact, the concept of potential SMC, i.e., PSMC, is introduced. At time n, a PSMC $\boldsymbol{y}_{k,n}$, $k \in \mathcal{K}_n \triangleq \{1, \ldots, K_n\}$ is either a legacy PSMC $\tilde{\boldsymbol{y}}_{k,n}$, which is already established in the previous time, or a new PSMC $\breve{\boldsymbol{y}}_{m,n}$ which is established for the first time. The existence/nonexistence of a PSMC as an actual SMC is modeled by a binary variable $r_{k,n} \in \{0, 1\}$, i.e., it exists (not exist) if $r_{k,n} = 1$ ($r_{k,n} = 0$). Thus, the number of PSMCs K_n represents the maximum possible number of SMCs that can be detected and estimated at time n.

The augmented state of a PSMC is defined as $\boldsymbol{y}_{k,n} \triangleq [\boldsymbol{\psi}_{k,n}, r_{k,n}]^\mathrm{T}$, where $\boldsymbol{\psi}_{k,n} = [\boldsymbol{x}_{k,n}^\mathrm{T}, u_{k,n}]^\mathrm{T}$ and $\boldsymbol{x}_{k,n} = [d_{k,n}, \varphi_{k,n}, v_{\mathrm{d},k,n}, v_{\varphi,k,n}]^\mathrm{T}$ with $v_{\mathrm{d},k,n}$ and $v_{\varphi,k,n}$ denoting the distance and angular velocities. The states of nonexisting PSMCs are obviously irrelevant, but will be convenient if formally considered. Therefore, all probability density functions (pdfs) defined for PSMC states $f(\boldsymbol{y}_{k,n}) = f(\boldsymbol{\psi}_{k,n}, r_{k,n})$ have the property that $f(\boldsymbol{\psi}_{k,n}, r_{k,n} = 0) = f_{k,n} f_\mathrm{D}(\boldsymbol{\psi}_{k,n})$, where $f_{k,n}$ is a constant representing the probability of nonexistence of $\boldsymbol{y}_{k,n}$, and $f_\mathrm{D}(\boldsymbol{\psi}_{k,n})$ is an arbitrary "dummy pdf" [21], [27]. Accordingly, the augmented states of legacy PSMCs and new PSMCs are denoted by $\tilde{\boldsymbol{y}}_{k,n} \triangleq [\tilde{\boldsymbol{\psi}}_{k,n}^\mathrm{T}, \tilde{r}_{k,n}]^\mathrm{T}$, $k \in \mathcal{K}_{n-1} \triangleq \{1, \ldots, K_{n-1}\}$ and $\breve{\boldsymbol{y}}_{m,n} \triangleq [\breve{\boldsymbol{\psi}}_{m,n}^\mathrm{T}, \breve{r}_{m,n}]^\mathrm{T}$, $m \in \mathcal{M}_n \triangleq \{1, \ldots, M_n\}$, respectively. At each time n, one new PSMC $\breve{\boldsymbol{y}}_{m,n}$ is introduced for each measurement $\boldsymbol{z}_{m,n}$, thus the number of new PSMCs equals to the number of measurements M_n. Before the current measurements $\boldsymbol{z}_n$ are observed, the number M_n is random. The new PSMCs become legacy PSMCs when the measurements at next time are observed, accordingly the set and number of legacy PSMCs are updated as $\mathcal{K}_n = \mathcal{K}_{n-1} \cup \mathcal{M}_n$ and $K_n =$

[1] An extension to three dimensional scenarios with horizontal and vertical propagation is straightforward, but it would lead to a cumbersome notation and one would not gain any new insights.

$K_{n-1} + M_n$. We further define the stacked state vectors as follows: for legacy PSMCs $\tilde{\boldsymbol{y}} \triangleq [\tilde{\boldsymbol{y}}_1^{\mathrm{T}}, \ldots, \tilde{\boldsymbol{y}}_n^{\mathrm{T}}]^{\mathrm{T}}$, $\tilde{\boldsymbol{y}}_n \triangleq [\tilde{\boldsymbol{y}}_{1,n}^{\mathrm{T}}, \ldots, \tilde{\boldsymbol{y}}_{K_{n-1},n}^{\mathrm{T}}]^{\mathrm{T}}$, $\tilde{\boldsymbol{x}}_n \triangleq [\tilde{\boldsymbol{x}}_{1,n}^{\mathrm{T}}, \ldots, \tilde{\boldsymbol{x}}_{K_{n-1},n}^{\mathrm{T}}]^{\mathrm{T}}$, $\tilde{\boldsymbol{u}}_n \triangleq [\tilde{u}_{1,n}, \ldots, \tilde{u}_{K_{n-1},n}]^{\mathrm{T}}$, $\tilde{\boldsymbol{r}}_n \triangleq [\tilde{r}_{1,n}, \ldots, \tilde{r}_{K_{n-1},n}]^{\mathrm{T}}$; for new PSMCs $\breve{\boldsymbol{y}}_n \triangleq [\breve{\boldsymbol{y}}_{1,n}^{\mathrm{T}}, \ldots, \breve{\boldsymbol{y}}_{M_n,n}^{\mathrm{T}}]^{\mathrm{T}}$, $\breve{\boldsymbol{x}}_n \triangleq [\breve{\boldsymbol{x}}_{1,n}^{\mathrm{T}}, \ldots, \breve{\boldsymbol{x}}_{M_n,n}^{\mathrm{T}}]^{\mathrm{T}}$, $\breve{\boldsymbol{u}}_n \triangleq [\breve{u}_{1,n}, \ldots, \breve{u}_{M_n,n}]^{\mathrm{T}}$, $\breve{\boldsymbol{r}}_n \triangleq [\breve{r}_{1,n}, \ldots, \breve{r}_{M_n,n}]^{\mathrm{T}}$; for combination of the legacy and new PSMCs, $\boldsymbol{y}_n \triangleq [\tilde{\boldsymbol{y}}_n^{\mathrm{T}}, \breve{\boldsymbol{y}}_n^{\mathrm{T}}]^{\mathrm{T}}$, $\boldsymbol{y}_n \triangleq [\boldsymbol{y}_{1,n}^{\mathrm{T}}, \ldots, \boldsymbol{y}_{K_n,n}^{\mathrm{T}}]^{\mathrm{T}}$ with $k \in \mathcal{K}_n \triangleq \{1, \ldots, K_n\}$.

Assume that the states $\tilde{\boldsymbol{y}}_{k,n}$ with $k \in \mathcal{K}_n$ of the legacy PSMCs are distributed independently across k and n, and evolve independently according to their respective Markovian state dynamics. The state-transition pdf for legacy PSMC state $\tilde{\boldsymbol{y}}_n$ factorizes as

$$f(\tilde{\boldsymbol{y}}_n|\boldsymbol{y}_{n-1}) = \prod_{k=1}^{K_{n-1}} f(\tilde{\boldsymbol{y}}_{k,n}|\boldsymbol{y}_{k,n-1}), \tag{3}$$

where $f(\tilde{\boldsymbol{y}}_{k,n}|\boldsymbol{y}_{k,n-1}) = f(\tilde{\boldsymbol{\psi}}_{k,n}, \tilde{r}_{k,n}|\boldsymbol{\psi}_{k,n-1}, r_{k,n-1})$ is the single PSMC state-transition pdf. If the PSMC did not exist at time $n-1$, i.e., $r_{k,n-1} = 0$, it cannot exist at time n as a legacy PSMC. This means that

$$f(\tilde{\boldsymbol{\psi}}_{k,n}, \tilde{r}_{k,n}|\boldsymbol{\psi}_{k,n-1}, 0) = \begin{cases} f_{\mathrm{D}}(\tilde{\boldsymbol{\psi}}_{k,n}), & \tilde{r}_{k,n} = 0 \\ 0, & \tilde{r}_{k,n} = 1\,. \end{cases} \tag{4}$$

If the PSMC existed at time $n-1$, i.e., $r_{k,n-1} = 1$, it either dies i.e., $\tilde{r}_{k,n} = 0$ or it still exist i.e., $\tilde{r}_{k,n} = 1$ with the survival probability denoted as P_{s}. If it does survive, the state $\tilde{\boldsymbol{\psi}}_{k,n}$ is distributed according to the state-transition pdf $f(\tilde{\boldsymbol{\psi}}_{k,n}|\boldsymbol{\psi}_{k,n-1})$. Thus we have

$$f(\tilde{\boldsymbol{\psi}}_{k,n}, \tilde{r}_{k,n}|\boldsymbol{\psi}_{k,n-1}, 1) = \begin{cases} (1-P_{\mathrm{s}}) f_{\mathrm{D}}(\tilde{\boldsymbol{\psi}}_{k,n}), & \tilde{r}_{k,n} = 0 \\ P_{\mathrm{s}} f(\tilde{\boldsymbol{\psi}}_{k,n}|\boldsymbol{\psi}_{k,n-1}), & \tilde{r}_{k,n} = 1\,. \end{cases} \tag{5}$$

We further factorize the state-transition pdfs as $f(\tilde{\boldsymbol{\psi}}_{k,n}|\boldsymbol{\psi}_{k,n-1}) = f(\tilde{\boldsymbol{x}}_{k,n}|\boldsymbol{x}_{k,n-1}) f(\tilde{u}_{k,n}|u_{k,n-1})$ given the independence assumptions between that the state vectors $\tilde{\boldsymbol{x}}_{k,n}$ and the normalized amplitudes $\tilde{u}_{k,n}$.

B. Associations of PSMCs with Measurements

The association of PSMCs and measurements is complicated by the DA uncertainty: at time n it is unknown which measurement $\boldsymbol{z}_{m,n}$ originates from which PSMC, or if a measurement did not originate from a PSMC (false alarm or clutter), or if a PSMC did not generate any measurement (missed detection). Any PSMC-to-measurement association is described by PSMC-oriented variables

$$a_{k,n} \triangleq \begin{cases} m \in \mathcal{M}_n, & \text{if the legacy PSMC } k \text{ generate the measurement } m \\ 0 & \text{if the legacy PSMC } k \text{ does not generate any measurement,} \end{cases}$$

stacked into the PSMC-oriented association vector $\boldsymbol{a}_n \triangleq [a_{1,n}, \ldots, a_{K_{n-1},n}]^{\mathrm{T}}$. To reduce computational complexity, following [8], [21], [27], we use a redundant description of PMSC-measurement associations, i.e., we introduce

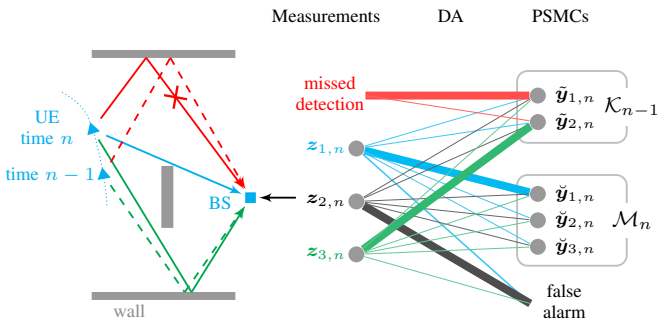

Fig. 1: An example of probabilistic DA, where the association probability between a measurement and a PSMC is denoted with the line thickness. At time n, three measurements are generated from the SBL channel estimator. The probability that the measurement $\boldsymbol{z}_{1,n}$ is associated with the new PSMC $\breve{\boldsymbol{y}}_{1,n}$ is much higher than the probability that $\boldsymbol{z}_{1,n}$ is associated with a legacy PSMC. The measurement $\boldsymbol{z}_{3,n}$ is associated with the legacy PSMC $\tilde{\boldsymbol{y}}_{2,n}$ with high probability. Besides, it is highly possible that the measurement $\boldsymbol{z}_{2,n}$ is a false alarm and the legacy PSMC $\tilde{\boldsymbol{y}}_{1,n}$ did not generate any measurement (missed detection).

measurement-oriented association variables

$$b_{m,n} \triangleq \begin{cases} k \in \mathcal{K}_{n-1}, & \text{if the measurement } m \text{ is generated by the legacy PSMC } k \\ 0 & \text{if the measurement } m \text{ is not generated by any legacy PSMC,} \end{cases}$$

and define the measurement-oriented association vector $\boldsymbol{b}_n \triangleq [b_{1,n}, \ldots, b_{M_n,n}]^{\mathrm{T}}$. Note that the "redundant formulation" of using $\boldsymbol{a}_n$ together with $\boldsymbol{b}_n$ is the key to make the algorithm scalable to the varying numbers of PSMCs and measurements.

The example presented in Fig. 1 explains how the probabilistic DA is performed. The probabilities of all association hypotheses of PSMCs and measurements are evaluated, and a high probability indicates that the PSMC state explains a measurement well.

C. States of Unknown Parameters

The detection and estimation of PSMC states require the information of the spatial density of false alarm measurements, and the detection probabilities, i.e., the probability that a PSMC $\boldsymbol{y}_{k,n}$ generates a measurement $\boldsymbol{z}_{m,n}$. We assume that the false alarm measurements are independent and identically distributed (iid) according to the pdf $f_{\mathrm{c}}(\boldsymbol{z}_{m,n})$, which is uniform on the region of interest (RoI), and the number of false alarm measurements at each time n, i.e., false alarm rate (FAR), is Poisson distributed with mean $\mu_{\mathrm{FA},n}$. The detection probability $P_{\mathrm{d}}(\boldsymbol{\psi}_{k,n}) \triangleq P_{\mathrm{d}}(u_{k,n})$ is characterized by its normalized amplitude [23], [24]. Both $\mu_{\mathrm{FA},n}$ and $P_{\mathrm{d}}(u_{k,n})$ are assumed to be unknown and potentially time-varying, and the algorithm is designed to automatically adapt these parameters online. More specifically, $\mu_{\mathrm{FA},n}$ is estimated continually along with the PSMC states, and $P_{\mathrm{d}}(u_{k,n})$ is given at each time by using the normalized amplitudes $u_{k,n}$, as explained in [23], [24] and Section III-D. The mean FAR $\mu_{\mathrm{FA},n}$ is independent of the states of the legacy PSMCs, and evolve according to the state-transition pdf $f(\mu_{\mathrm{FA},n}|\mu_{\mathrm{FA},n-1})$.

D. Likelihood Functions

If the measurement $\boldsymbol{z}_{m,n}$ is originated from the PSMC k, i.e., $a_{k,n} = m$, then the conditional distribution given the state $\boldsymbol{\psi}_{k,n}$ is described by the pdf $f(\boldsymbol{z}_{m,n}|\boldsymbol{\psi}_{k,n})$. Assuming the individual measurements inside vector $\boldsymbol{z}_{m,n}$ are conditional independent given the state $\boldsymbol{\psi}_{k,n}$, the pdfs $f(\boldsymbol{z}_{m,n}|\boldsymbol{\psi}_{k,n})$ of PSMC-originated measurements factorizes as

$$f(\boldsymbol{z}_{m,n}|\boldsymbol{\psi}_{k,n}) = f(\hat{d}_{m,n}|d_{k,n})f(\hat{\varphi}_{m,n}|\varphi_{k,n})f(\hat{u}_{m,n}|u_{k,n}), \quad (6)$$

where the conditional pdfs $f(\hat{d}_{m,n}|d_{k,n})$ and $f(\hat{\varphi}_{m,n}|\varphi_{k,n})$ are defined by Gaussian measurement models, yields

$$f(\hat{d}_{m,n}|d_{k,n}) = \frac{1}{\sqrt{2\pi\sigma^2_{\mathrm{d},m,n}}} \exp\big(\frac{-(\hat{d}_{m,n} - d_{k,n})^2}{2\sigma^2_{\mathrm{d},m,n}}\big), \quad (7)$$

$$f(\hat{\varphi}_{m,n}|\varphi_{k,n}) = \frac{1}{\sqrt{2\pi\sigma^2_{\varphi,m,n}}} \exp\big(\frac{-(\hat{\varphi}_{m,n} - \varphi_{k,n})^2}{2\sigma^2_{\varphi,m,n}}\big). \quad (8)$$

The variances are computed using the norm amplitude measurements, i.e., $\sigma^2_{\mathrm{d},m,n} = c^2/(8\pi^2\beta_{\mathrm{bw}}\hat{u}^2_{m,n})$ and $\sigma^2_{\varphi,m,n} = c^2/(8\pi^2 f_{\mathrm{c}}^2\hat{u}^2_{m,n}D^2(\hat{\varphi}_{m,n}))$, where β_{bw} is the mean square bandwidth of the transmit signal pulse $s(t)$ and $D^2(\hat{\varphi}_{m,n})$ is the squared array aperture [24], [26]. The pdf $f(\hat{u}_{m,n}|u_{k,n})$ of the normalized amplitude $\hat{u}_{m,n}$ conditioned on the state $u_{k,n}$ is given by a unit-variance Rician distribution as in [23], [24].

If $\boldsymbol{z}_{m,n}$ is a false alarm measurement, it is distributed according to the pdf $f_{\mathrm{FA}}(\boldsymbol{z}_{m,n})$, which factorizes as

$$f_{\mathrm{FA}}(\boldsymbol{z}_{m,n}) = f_{\mathrm{FA}}(\hat{d}_{m,n})f_{\mathrm{FA}}(\hat{\varphi}_{m,n})f_{\mathrm{FA}}(\hat{u}_{m,n}), \quad (9)$$

where $f_{\mathrm{FA}}(\hat{d}_{m,n})$ and $f_{\mathrm{FA}}(\hat{\varphi}_{m,n})$ are assumed to be uniform in their respective RoIs, i.e., $f_{\mathrm{FA}}(\hat{d}_{m,n}) = 1/d_{\max}$ and $f_{\mathrm{FA}}(\hat{\varphi}_{m,n}) = 1/2\pi$. The false alarm pdf $f_{\mathrm{FA}}(\hat{u}_{m,n})$ of the normalized amplitude is given by a unit-variance Rayleigh distribution [20, Ch. 1.6.7], i.e., $f_{\mathrm{FA}}(\hat{u}_{m,n}) = \hat{u}_{m,n}\exp(-\hat{u}^2_{m,n}/2)/P_{\mathrm{FA}}$. The false alarm probability is given as $P_{\mathrm{FA}} = \exp(-u^2_{\mathrm{th}}/2)$ with the normalized amplitude threshold u_{th}.

E. Joint Posterior pdf and Factor Graph

By using common assumptions [8], [21], and for fixed and thus observed measurements $\boldsymbol{z}$, it can be shown that the joint posterior pdf of $\tilde{\boldsymbol{y}}$, $\breve{\boldsymbol{y}}$, $\boldsymbol{a}$, $\boldsymbol{b}$, $\boldsymbol{\mu}_{\mathrm{FA}}$ and $\boldsymbol{m}$, conditioned on $\boldsymbol{z}$ is given by

$$\begin{aligned} &f(\tilde{\boldsymbol{y}}, \breve{\boldsymbol{y}}, \boldsymbol{a}, \boldsymbol{b}, \boldsymbol{\mu}_{\mathrm{FA}}, \boldsymbol{m}|\boldsymbol{z}) \\ &\propto f(\mu_{\mathrm{FA},1}) \prod_{m'=1}^{M_1} h(\breve{\boldsymbol{\psi}}_{m',1}, \breve{r}_{m',1}, b_{m',1}, \mu_{\mathrm{FA},1}; \boldsymbol{z}_1) \\ &\quad \times \prod_{n'=2}^{n} f(\mu_{\mathrm{FA},n'}|\mu_{\mathrm{FA},n'-1}) \left(\prod_{k=1}^{K_{n'-1}} f(\tilde{\boldsymbol{y}}_{k,n'}|\boldsymbol{y}_{k,n'-1}) \right) \\ &\quad \times \left(\prod_{k=1}^{K_{n'-1}} \prod_{m=1}^{M_{n'}} g(\tilde{\boldsymbol{y}}_{k,n'}, a_{k,n'}, \mu_{\mathrm{FA},n'}; \boldsymbol{z}_{n'}) \Psi(a_{k,n'}, b_{m,n'}) \right) \\ &\quad \times \left(\prod_{m=1}^{M_{n'}} f(\breve{\boldsymbol{y}}_{m,n'}) h(\breve{\boldsymbol{y}}_{m,n'}, b_{m,n'}, \mu_{\mathrm{FA},n'}; \boldsymbol{z}_{n'}) \right), \end{aligned} \quad (10)$$

where we introduced the functions $g(\tilde{\boldsymbol{y}}_{k,n}, a_{k,n}, \mu_{\mathrm{FA},n}; \boldsymbol{z}_n)$, $h(\breve{\boldsymbol{y}}_{m,n}, b_{m,n}, \mu_{\mathrm{FA},n}; \boldsymbol{z}_n)$, $f(\breve{\boldsymbol{y}}_{m,n})$, and $\Psi(a_{k,n}, b_{m,n})$ that will be discussed next.

The pseudo likelihood functions are given as $g(\tilde{\boldsymbol{y}}_{k,n}, a_{k,n}, \mu_{\mathrm{FA},n}; \boldsymbol{z}_n) = g(\tilde{\boldsymbol{\psi}}_{k,n}, \tilde{r}_{k,n}, a_{k,n}, \mu_{\mathrm{FA},n}; \boldsymbol{z}_n)$ and $h(\breve{\boldsymbol{y}}_{m,n}, b_{m,n}, \mu_{\mathrm{FA},n}; \boldsymbol{z}_n) = h(\breve{\boldsymbol{\psi}}_{m,n}, \breve{r}_{m,n}, b_{m,n}, \mu_{\mathrm{FA},n}; \boldsymbol{z}_n)$

$$\begin{aligned} &g(\tilde{\boldsymbol{\psi}}_{k,n}, 1, a_{k,n}, \mu_{\mathrm{FA},n}; \boldsymbol{z}_n) \\ &= \begin{cases} \dfrac{n(\mu_{\mathrm{FA},n}) f(\boldsymbol{z}_{m,n}|\tilde{\boldsymbol{\psi}}_{k,n}) P_{\mathrm{d}}(\tilde{u}_{k,n})}{\mu_{\mathrm{FA},n} f_{\mathrm{FA}}(\boldsymbol{z}_{m,n})}, & a_{k,n} = m \in \mathcal{M}_n \\ 1 - P_{\mathrm{d}}(\tilde{u}_{k,n}), & a_{k,n} = 0, \end{cases} \end{aligned} \quad (11)$$

and $g(\tilde{\boldsymbol{\psi}}_{k,n}, 0, a_{k,n}, \mu_{\mathrm{FA},n}; \boldsymbol{z}_n) = 1(a_{k,n})n(\mu_{\mathrm{FA},n})$ with $n(\mu_{\mathrm{FA},n}) \triangleq (\mu^{M_n}_{\mathrm{FA},n} e^{-\mu_{\mathrm{FA},n}}/M_n!)^{1/(K_{n-1}+M_n)}$ as well as

$$\begin{aligned} &h(\breve{\boldsymbol{\psi}}_{m,n}, 1, b_{m,n}, \mu_{\mathrm{FA},n}; \boldsymbol{z}_n) \\ &= \begin{cases} 0, & b_{m,n} = k \in \mathcal{K}_{n-1} \\ \dfrac{n(\mu_{\mathrm{FA},n}) f(\boldsymbol{z}_{m,n}|\breve{\boldsymbol{\psi}}_{m,n})}{\mu_{\mathrm{FA},n} f_{\mathrm{FA}}(\boldsymbol{z}_{m,n})}, & b_{m,n} = 0, \end{cases} \end{aligned} \quad (12)$$

and $h(\breve{\boldsymbol{\psi}}_{m,n}, 0, b_{m,n}, \mu_{\mathrm{FA},n}; \boldsymbol{z}_n) = n(\mu_{\mathrm{FA},n})$. The prior distributions $f(\breve{\boldsymbol{y}}_{m,n}) = f(\breve{\boldsymbol{\psi}}_{m,n}, \breve{r}_{m,n})$ for new PSMC states can be expressed as

$$f(\breve{\boldsymbol{\psi}}_{m,n}, \breve{r}_{m,n}) = \begin{cases} \mu_{\mathrm{n}} f_{\mathrm{n}}(\breve{\boldsymbol{\psi}}_{m,n}), & \breve{r}_{m,n} = 1 \\ f_{\mathrm{D}}(\breve{\boldsymbol{\psi}}_{m,n}), & \breve{r}_{m,n} = 0, \end{cases} \quad (13)$$

where μ_{n} and $f_{\mathrm{n}}(\breve{\boldsymbol{\psi}}_{m,n})$ are the mean and pdf of a Poisson point process, respectively. Finally, the binary indicator functions that check consistency for any pair $(a_{k,n}, b_{m,n})$ of PSMC-oriented and measurement-oriented association variable at time n, read [8], [21]

$$\Psi(a_{k,n}, b_{m,n}) = \begin{cases} 0, & a_{k,n} = m, b_{m,n} \neq k \\ & \text{or } b_{m,n} = k, a_{k,n} \neq m \\ 1, & \text{otherwise.} \end{cases} \quad (14)$$

In case the joint PSMC-oriented association vector $\boldsymbol{a}_n$ and the measurement-oriented association vector $\boldsymbol{b}_n$ do not describe the same association event, at least one indicator function in (10) is zero and thus $f(\tilde{\boldsymbol{y}}, \breve{\boldsymbol{y}}, \boldsymbol{a}, \boldsymbol{b}, \boldsymbol{\mu}_{\mathrm{FA}}, \boldsymbol{m}|\boldsymbol{z})$ is zero as well. The factor graph describing the factorization (10) of the joint posterior pdf is shown in Fig. 2.

IV. The BP-based MPC Tracking algorithm

In the Bayesian setting, the detection of PSMCs $\boldsymbol{y}_{k,n}$ with $k \in \mathcal{K}_n$ relies on the marginal posterior existence probabilities $f(r_{k,n} = 1|\boldsymbol{z})$, and the estimation of the detected PSMC states $\boldsymbol{x}_{k,n}$, the amplitudes $u_{k,n}$ and the mean FAR $\mu_{\mathrm{FA},n}$ rely on the marginal posterior pdfs $f(\boldsymbol{\psi}_{k,n}|r_{k,n} = 1, \boldsymbol{z})$ and $f(\mu_{\mathrm{FA},n}|\boldsymbol{z})$. More specifically, a PSMC is detected if $p(r_{n,k} = 1|\boldsymbol{z}) > P_{\mathrm{det}}$ [28], where $p(r_{n,k} = 1|\boldsymbol{z})$ is obtained

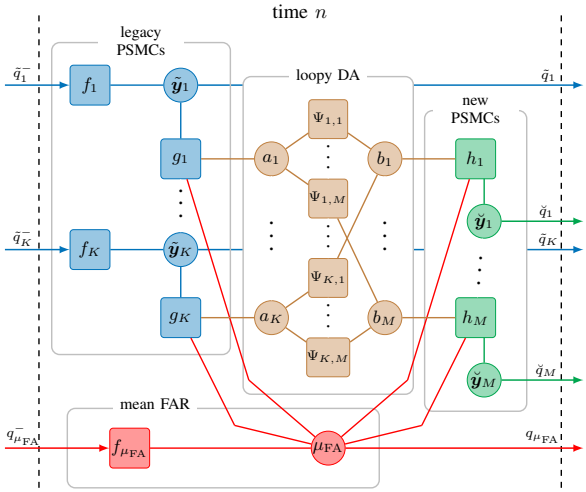

Fig. 2: Factor graph representation of the factorized joint posterior pdf (10), shown for time n. For simplicity, the following short notations are used: $K \triangleq K_{n-1}$, $M \triangleq M_n$; *variable nodes*: $a_k \triangleq a_{k,n}$, $b_m \triangleq b_{m,n}$, $\mu_{\text{FA}} \triangleq \mu_{\text{FA},n}$, $\tilde{\boldsymbol{y}}_k \triangleq \tilde{\boldsymbol{y}}_{k,n}$, $\breve{\boldsymbol{y}}_m \triangleq \breve{\boldsymbol{y}}_{m,n}$; *factor nodes*: $f_k \triangleq f(\tilde{\boldsymbol{y}}_{k,n}|\boldsymbol{y}_{k,n-1})$, $f_{\mu_{\text{FA}}} \triangleq f(\mu_{\text{FA},n}|\mu_{\text{FA},n-1})$, $g_k \triangleq g(\tilde{\boldsymbol{\psi}}_{k,n}, \tilde{r}_{k,n}, a_{k,n}, \mu_{\text{FA},n}; \boldsymbol{z}_n)$, $h_m \triangleq h(\breve{\boldsymbol{\psi}}_{m,n}, \breve{r}_{m,n}, b_{m,n}, \mu_{\text{FA},n}; \boldsymbol{z}_n)$, $\Psi_{k,m} \triangleq \Psi(a_{k,n}, b_{m,n})$; beliefs: $\tilde{q}_k^- \triangleq \tilde{q}(\tilde{\boldsymbol{\psi}}_{k,n-1}, \tilde{r}_{k,n-1})$, $\tilde{q}_k \triangleq \tilde{q}(\tilde{\boldsymbol{\psi}}_{k,n}, \tilde{r}_{k,n})$, $\breve{q}_m \triangleq \breve{q}(\breve{\boldsymbol{\psi}}_{m,n}, \breve{r}_{m,n})$, $q_{\mu_{\text{FA}}}^- \triangleq q(\mu_{\text{FA},n-1})$, $q_{\mu_{\text{FA}}} \triangleq q(\mu_{\text{FA},n})$.

from the marginal posterior pdfs of the augmented PSMC state $f(\boldsymbol{y}_{k,n}|\boldsymbol{z}) = f(\boldsymbol{\psi}_{k,n}, r_{k,n}|\boldsymbol{z})$ as

$$p(r_{k,n}=1|\boldsymbol{z}) = \int f(\boldsymbol{\psi}_{k,n}, r_{k,n}=1|\boldsymbol{z})\mathrm{d}\boldsymbol{\psi}_{k,n}. \tag{15}$$

The estimates of $\mu_{\text{FA},n}$, and the states $\boldsymbol{\psi}_{k,n}$ and $u_{k,n}$ of detected PSMCs are calculated by means of the minimum mean-square error (MMSE) estimator [29]

$$\hat{\mu}_{\text{FA},n}^{\text{MMSE}} \triangleq \int \mu_{\text{FA},n} f(\mu_{\text{FA},n}|\boldsymbol{z})\mathrm{d}\mu_{\text{FA},n}, \tag{16}$$

$$\hat{\boldsymbol{x}}_{k,n}^{\text{MMSE}} \triangleq \int \boldsymbol{x}_{k,n} f(\boldsymbol{\psi}_{k,n}|r_{k,n}=1,\boldsymbol{z})\mathrm{d}\boldsymbol{\psi}_{k,n}, \tag{17}$$

$$\hat{u}_{k,n}^{\text{MMSE}} \triangleq \int u_{k,n} f(\boldsymbol{\psi}_{k,n}|r_{k,n}=1,\boldsymbol{z})\mathrm{d}\boldsymbol{\psi}_{k,n}, \tag{18}$$

where the marginal posterior pdf $f(\boldsymbol{\psi}_{k,n}|r_{k,n}=1,\boldsymbol{z})$ can be obtained from $f(\boldsymbol{\psi}_{k,n}, r_{k,n}|\boldsymbol{z})$ as

$$f(\boldsymbol{\psi}_{k,n}|r_{k,n}=1,\boldsymbol{z}) = \frac{f(\boldsymbol{\psi}_{k,n}, r_{k,n}=1|\boldsymbol{z})}{f(r_{k,n}=1|\boldsymbol{z})}. \tag{19}$$

Note that the posterior existence probabilities $f(r_{k,n}=1|\boldsymbol{z})$ are also used in the pruning step removing PSMCs with $f(r_{k,n}=1|\boldsymbol{z}_{1:n}) < P_{\text{prun}}$. As explained in Section III-A, the number of legacy PSMCs are updated as $K_n = K_{n-1}+M_n$ at each time n, the pruning step would prevent K_n from growing indefinitely.

To obtain the marginal posterior pdfs $f(\tilde{\boldsymbol{\psi}}_{k,n}, \tilde{r}_{k,n}|\boldsymbol{z})$, $f(\breve{\boldsymbol{\psi}}_{m,n}, \breve{r}_{m,n}|\boldsymbol{z})$ and $f(\mu_{\text{FA},n}|\boldsymbol{z})$ of the join posterior pdf $f(\tilde{\boldsymbol{y}}, \breve{\boldsymbol{y}}, \boldsymbol{a}, \boldsymbol{b}, \boldsymbol{\mu}_{\text{FA}}, \boldsymbol{m}|\boldsymbol{z})$, direct marginalization is infeasible. However, their respective approximations $\tilde{q}(\tilde{\boldsymbol{y}}_{k,n}) = \tilde{q}(\tilde{\boldsymbol{\psi}}_{k,n}, \tilde{r}_{k,n})$, $\breve{q}(\breve{\boldsymbol{y}}_{m,n}) = \breve{q}(\breve{\boldsymbol{\psi}}_{m,n}, \breve{r}_{m,n})$ and $q(\mu_{\text{FA},n})$ can be obtained efficiently by running the iterative BP [30] on the factor graph in Fig. 2. Since this factor graph is loopy, we now specify the following order in which the message are computed: (i) messages are not sent backward in time; (ii) iterative message passing is only performed for probabilistic DA at each time step. In addition, the generic BP rules for calculating messages and beliefs introduced in [21, Ch. III] are also followed. A sequential particle-based message passing implementation [8], [21], [27] is used to approximate the messages and beliefs.

V. Experimental Results

The proposed BP-MPCT algorithm is validated using synthetic channel measurement data. Given the floor plan of a seminar room at Graz University of Technology [8], the true SMC parameters and model order are firstly obtained by using a ray tracing (RT) method, and then applied in the radio signal model (2) to synthetically generate the channel measurement data for each simulation run. We assume that the amplitude of each SMC follows free-space pathloss and is attenuated by 3 dB after each reflection. The transmit pulse $s(t)$ is a root-raised-cosine pulse with a symbol duration $T_{\text{p}} = 2\,\text{ns}$ and a roll-off factor of 0.6 at a center frequency of $f_{\text{c}} = 6\,\text{GHz}$ with bandwidth of 500 MHz. The number of samples $N_{\text{s}} = 94$. A 3×3 uniform rectangular array with an inter-element spacing of 1 cm is used at the BS. The true SNR of a MPC is computed as $\text{SNR}_{l,n} = 10\log_{10}(\frac{|\alpha_{l,n}|^2\|\boldsymbol{s}(\boldsymbol{\theta}_{l,n})\|^2 T_s}{N_0})$. For each simulation run, the AWGN is generated with the noise variance $\sigma_{\text{w}}^2 = N_0/T_s$ specified with a given $\text{SNR}_{\text{lm}} = 10\log_{10}(\frac{|\alpha_{\text{LOS}}|^2\|\boldsymbol{s}_{\text{LOS}}\|^2 T_s}{N_0})$, where the amplitude α_{LOS} and the signal vector $\boldsymbol{s}_{\text{LOS}}$ from all array elements of the line-of-sight (LOS) component are computed at 1 m distance. The synthetic channel measurement data is used in the SBL channel estimator to obtain the noisy measurements $\boldsymbol{z}_{m,n}$ at each time n, and the true number of false alarm measurements is obtained by checking the optimal sub-pattern assignment (OSPA) matrix [31] between $\boldsymbol{z}_{m,n}$ and the true SMC parameters from RT. Note that we on purposely generated more false alarm measurements by setting the detection threshold (on individual MPC's SNR) to 8 dB in the SBL channel estimator, which is smaller than the threshold according to [18], therefore the performance of the BP-MPCT algorithm can be validated in more challenging situations. In total, we performed 50 simulation runs for each given $\text{SNR}_{\text{lm}} \in \{25\,\text{dB}, 30\,\text{dB}, 35\,\text{dB}\}$. The parameters used in the BP-MPCT algorithm are as follows: the number of particles is 10000, the survival probability $P_{\text{s}} = 0.999$, the detection probability threshold $P_{\text{det}} = 0.5$, the pruning threshold $P_{\text{prun}} = 10^{-4}$, the mean number of newly detected SMCs $\mu_{\text{n}} = 0.01$, the birth pdf $f_{\text{n}}(\breve{\boldsymbol{\psi}}_{m,n})$ is uniform on the RoI, i.e., $f_{\text{n}}(\breve{\boldsymbol{\psi}}_{m,n}) = 1/(2\pi d_{\max})$ with $d_{\max} = 30\,\text{m}$. The P_{FA} is calculated for a threshold of $u_{\text{th}} = 1$. The detection probabilities $P_{\text{d}}(\hat{u}_{k,n}^{\text{MMSE}})$ are calculated using the MMSE estimates of the normalized amplitudes $\hat{u}_{k,n}^{\text{MMSE}}$ [23]. The particles for the initial mean FAR are drawn from a uniform distribution on $[0.001, 15]$. The particles for the initial states $\breve{\boldsymbol{\psi}}_{m,n}$ of a new PSMC are drawn from a 5-

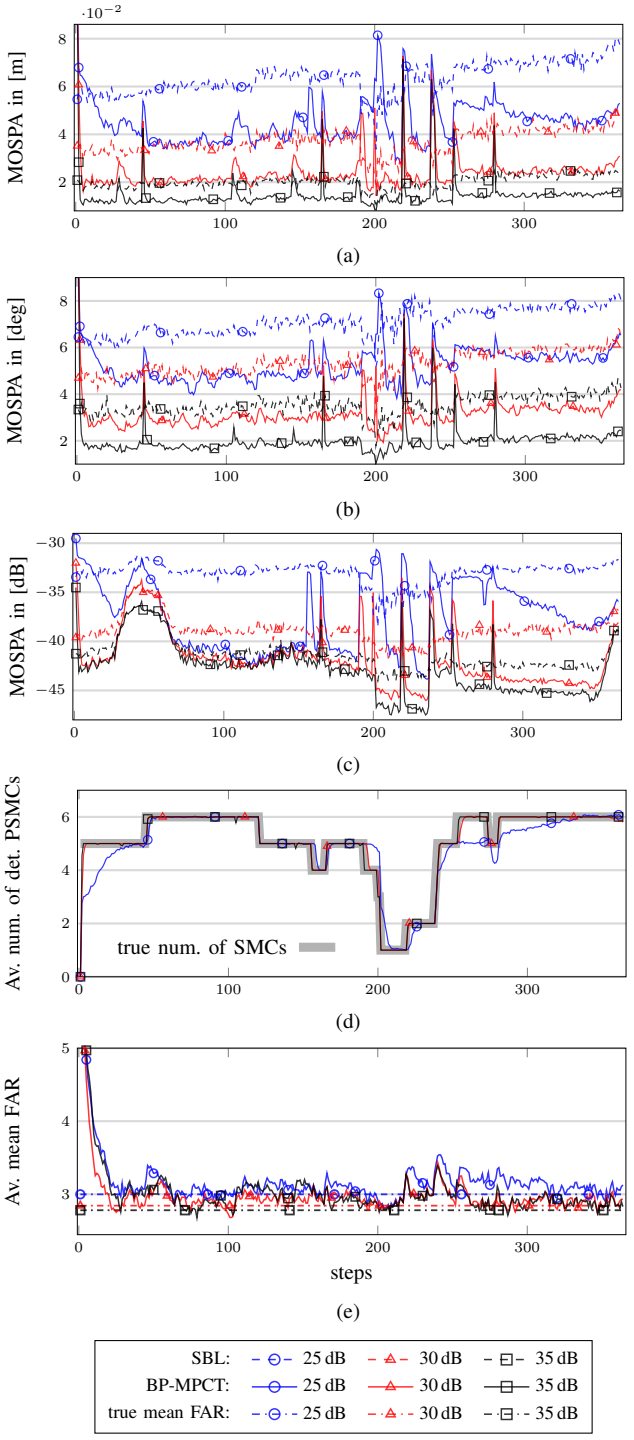

Fig. 3: For different $\mathrm{SNR}_{1\mathrm{m}}$, MOSPA errors on (a) distances, (b) AoAs, and (c) amplitudes. (d) Averaged number of detected PSMCs. (e) Averaged estimated mean FAR.

D uniform distribution with center at $[\hat{d}_{m,n}, \hat{\varphi}_{m,n}, 0, 0, \hat{u}_{m,n}]$ and the support of each component is given by: $[-0.3, 0.3]$ m, $[-0.7, 0.7]$ rad, $[-0.01, 0.01]$ m/s, $[-0.01, 0.01]$ rad/s, $[-1, 1]$. The state-transition pdf of $\boldsymbol{x}_{k,n}$ is defined by a nearly-constant velocity model [32, Section 6.3.2] with $\Delta T = 1\,\mathrm{s}$ and noise standard deviations $\sigma_{\mathrm{d}} = 0.01\,\mathrm{m/s^2}$ and $\sigma_{\varphi} = 0.02\,\mathrm{rad/s^2}$ for distance and AoA, respectively. Furthermore, the state-transition pdfs of the normalized amplitude $f(u_{k,n}|u_{k,n-1})$ and the mean FAR $f(\mu_{\mathrm{FA},n}|\mu_{\mathrm{FA},n-1})$ are given as Gaussian distributions with noise standard deviations $\sigma_u = 1$ and $\sigma_{\mathrm{FAR}} = 0.4$, respectively.

The results of the BP-MPCT algorithm after averaging over 50 simulation runs are presented in Fig. 3, and the estimates $\boldsymbol{z}_{m,n}$ from the SBL estimator (after excluding the false alarm measurements) are used for comparison. It can be seen that the mean OSPA (MOSPA) [31] errors on the distances, AoAs and amplitudes obtained with BP-MPCT are mostly lower than the errors with SBL, and the advantage gets more obvious at low $\mathrm{SNR}_{1\mathrm{m}}$. This can be explained that: given low $\mathrm{SNR}_{1\mathrm{m}}$, there exist more "weak" SMCs with low SNRs that are sometimes miss detected in SBL, and some of the miss detections can be reconstructed in BP-MPCT, which leads to the better estimation of the model order and therefore lower MOSPA errors. Given the $\mathrm{SNR}_{1\mathrm{m}} = 35\,\mathrm{dB}$, the MOSPA errors obtained with BP-MPCT are mostly below 2 cm for distances, 2 degrees for AoAs and -40 dB for amplitudes. Furthermore, raises of the MOSPA errors for BP-MPCT are observed at time instances where the true number of SMCs changes, which happen mainly due to model order mismatch instead of the increases on the root mean square errors of individual detected PSMCs. More specifically, it takes one or two steps until the existence probabilities of the legacy/new PSMCs reach the detection probability threshold P_{det}, so tracks are terminated or newly detected, and therefore the change on the model order can be followed. As shown in Fig. 3d, the BP-MPCT algorithm is able to follow the correct model order for the most of the time, even for $\mathrm{SNR}_{1\mathrm{m}} = 25\,\mathrm{dB}$. Moreover, the estimated mean FAR converges to the true value regardless of the $\mathrm{SNR}_{1\mathrm{m}}$ condition as depicted in Fig. 3e.

The results of an exemplary simulation run given $\mathrm{SNR}_{1\mathrm{m}} = 25\,\mathrm{dB}$ are shown in Fig. 4. As can be seen, the BP-MPCT algorithm shows good ability to distinguish between false alarm measurements and measurements originated from SMCs. The birth-death processes of SMCs are accurately detected and tracks are well reconstructed even for some "weak" SMCs, for example, the estimated track denoted in cyan between time $n = 1$ and $n = 200$, of which the true SNR is mostly below the 8 dB detection threshold. Furthermore, the association of estimates over time in delay and angular subspaces are robust even in the presence of intersections between SMCs.

VI. Conclusions

We presented a BP-MPCT algorithm which jointly performs probabilistic DA, detection and tracking of MPC parameters. This algorithm is adaptive to time-varying mean false alarm rate, as well as the detection probabilities by utilizing the amplitude statistics of the MPC estimates. Simulation results showed that the BP-MPCT algorithm has excellent performance regarding the scalability to the time-varying model order, estimation accuracy, and association property over time in a realistic and very challenging scenario.

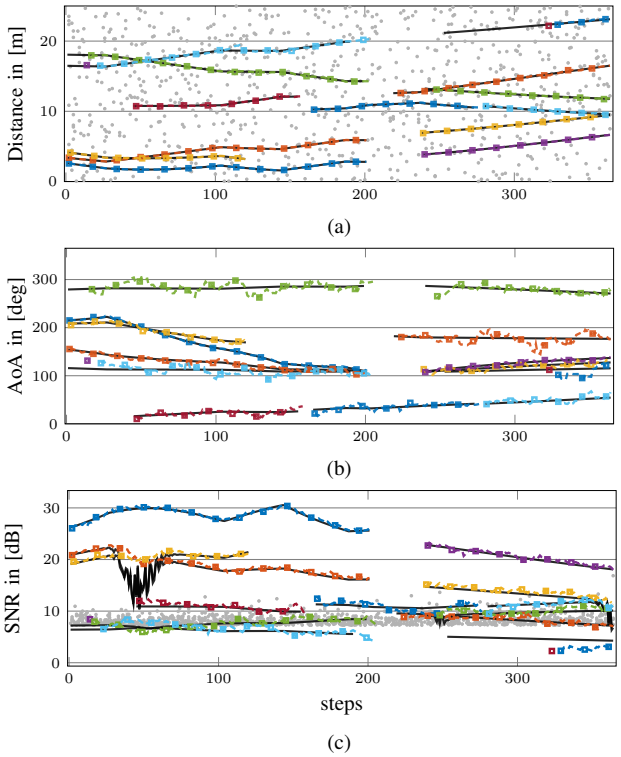

Fig. 4: Estimation results of a single simulation run for $\mathrm{SNR}_{1\mathrm{m}} = 25\,\mathrm{dB}$ on (a) distances, (b) AoAs, and (c) SNRs, i.e., the squares of the estimated normalized amplitudes. False alarm measurements are depicted by gray dots, true SMC parameters by black solid lines, and estimates of detected PSMCs by different colors.

VII. Acknowledgment

This work was supported in part by the Swedish Research Council (VR), in part by the strategic research area ELLIIT and in part by the TU Graz.

References

[1] M. L. Jakobsen, T. Pedersen, and B. H. Fleury, "Analysis of stochastic radio channels with temporal birth-death dynamics: A marked spatial point process perspective," *IEEE Trans. Antennas Propag.*, vol. 62, no. 7, pp. 3761–3775, Apr. 2014.

[2] J. Flordelis, X. Li, O. Edfors, and F. Tufvesson, "Massive MIMO extensions to the COST 2100 channel model: Modeling and validation," *IEEE Trans. Wireless Commun.*, vol. 19, no. 1, pp. 380–394, Oct. 2020.

[3] F. Rusek, D. Persson, B. K. Lau, E. G. Larsson, T. L. Marzetta, O. Edfors, and F. Tufvesson, "Scaling up MIMO: Opportunities and challenges with very large arrays," *IEEE Signal Process. Mag.*, vol. 30, no. 1, pp. 40–60, Jan. 2013.

[4] R. Di Taranto, S. Muppirisetty, R. Raulefs, D. Slock, T. Svensson, and H. Wymeersch, "Location-aware communications for 5G networks: How location information can improve scalability, latency, and robustness of 5G," *IEEE Signal Process. Mag.*, vol. 31, no. 6, pp. 102–112, Nov. 2014.

[5] S. Hu, F. Rusek, and O. Edfors, "Beyond massive MIMO: The potential of data transmission with large intelligent surfaces," *IEEE Trans. Signal Process.*, vol. 66, no. 10, pp. 2746–2758, May 2018.

[6] C. Gentner, T. Jost, W. Wang, S. Zhang, A. Dammann, and U. C. Fiebig, "Multipath assisted positioning with simultaneous localization and mapping," *IEEE Trans. Wireless Commun.*, vol. 15, no. 9, pp. 6104–6117, Sept. 2016.

[7] R. Mendrzik, F. Meyer, G. Bauch, and M. Z. Win, "Enabling situational awareness in millimeter wave massive MIMO systems," *IEEE J. Sel. Topics Signal Process.*, vol. 13, no. 5, pp. 1196–1211, Sept. 2019.

[8] E. Leitinger, F. Meyer, F. Hlawatsch, K. Witrisal, F. Tufvesson, and M. Z. Win, "A belief propagation algorithm for multipath-based SLAM," *IEEE Trans. Wireless Commun.*, vol. 18, no. 12, pp. 5613–5629, Dec. 2019.

[9] J. Salmi, A. Richter, and V. Koivunen, "Detection and tracking of MIMO propagation path parameters using state-space approach," *IEEE Trans. Signal Process.*, vol. 57, no. 4, pp. 1538–1550, Apr. 2009.

[10] X. Li, E. Leitinger, M. Oskarsson, K. Åström, and F. Tufvesson, "Massive MIMO-based localization and mapping exploiting phase information of multipath components," *IEEE Trans. Wireless Commun.*, vol. 18, no. 9, pp. 4254–4267, Sept. 2019.

[11] M. Haardt, F. Roemer, and G. Del Galdo, "Higher-order SVD-based subspace estimation to improve the parameter estimation accuracy in multidimensional harmonic retrieval problems," *IEEE Trans. Signal Process.*, vol. 56, no. 7, pp. 3198–3213, June 2008.

[12] D. Shutin and B. H. Fleury, "Sparse variational Bayesian SAGE algorithm with application to the estimation of multipath wireless channels," *IEEE Trans. Signal Proces.*, vol. 59, no. 8, pp. 3609–3623, Aug. 2011.

[13] A. Richter, "Estimation of radio channel parameters: Models and algorithms," Ph.D. dissertation, Ilmenau University of Technology, 2005.

[14] T. Jost, W. Wang, U.-C. Fiebig, and F. Perez-Fontan, "Detection and tracking of mobile propagation channel paths," *IEEE Trans. Antennas Propag.*, vol. 60, no. 10, pp. 4875–4883, Oct. 2012.

[15] F. Meyer, Y. Park, and P. Gerstoft, "Variational Bayesian estimation of time-varying DOAs," in *Proc. IEEE Fusion-20*, Rustenburg, South Africa, Sept. 2020, pp. 1–6.

[16] M. A. Badiu, T. L. Hansen, and B. H. Fleury, "Variational Bayesian inference of line spectra," *IEEE Trans. Signal Process.*, vol. 65, no. 9, pp. 2247–2261, May 2017.

[17] T. L. Hansen, B. H. Fleury, and B. D. Rao, "Superfast line spectral estimation," *IEEE Trans. Signal Process.*, vol. PP, no. 99, pp. 1–1, 2018.

[18] S. Grebien, E. Leitinger, K. Witrisal, and B. H. Fleury, "Super-resolution channel estimation including the dense multipath component — A sparse variational Bayesian approach," 2021, in preperation.

[19] D. Shutin and B. Vexler, "Sparse Bayesian learning with dictionary refinement for super-resolution through time," in *Proc. IEEE CAMSAP-17*, Dec. 2017, pp. 1–5.

[20] Y. Bar-Shalom, P. K. Willett, and X. Tian, *Tracking and data fusion: a handbook of algorithms*. Storrs, CT, USA: Yaakov Bar-Shalom, 2011.

[21] F. Meyer, T. Kropfreiter, J. L. Williams, R. Lau, F. Hlawatsch, P. Braca, and M. Z. Win, "Message passing algorithms for scalable multitarget tracking," *Proc. IEEE*, vol. 106, no. 2, pp. 221–259, Feb. 2018.

[22] D. Lerro and Y. Bar-Shalom, "Automated tracking with target amplitude information," in *1990 American Control Conf.*, May 1990, pp. 2875–2880.

[23] E. Leitinger, S. Grebien, X. Li, F. Tufvesson, and K. Witrisal, "On the use of MPC amplitude information in radio signal based SLAM," in *Proc. IEEE SSP-18*, Freiburg, Germany, June 2018, pp. 633–637.

[24] E. Leitinger, S. Grebien, and K. Witrisal, "Multipath-based SLAM exploiting AoA and amplitude information," in *Proc. IEEE ICCW-19*, Shanghai, China, May 2019, pp. 1–7.

[25] G. Soldi, F. Meyer, P. Braca, and F. Hlawatsch, "Self-tuning algorithms for multisensor-multitarget tracking using belief propagation," *IEEE Trans. Signal Process.*, vol. 67, no. 15, pp. 3922–3937, Aug. 2019.

[26] T. Wilding, S. Grebien, E. Leitinger, U. Mühlmann, and K. Witrisal, "Single-anchor, multipath-assisted indoor positioning with aliased antenna arrays," in *Asilomar-18*, Pacifc Grove, CA, USA, Oct. 2018, pp. 525–531.

[27] F. Meyer, P. Braca, P. Willett, and F. Hlawatsch, "A scalable algorithm for tracking an unknown number of targets using multiple sensors," *IEEE Trans. Signal Process.*, vol. 65, no. 13, pp. 3478–3493, July 2017.

[28] S. M. Kay, *Fundamentals of Statistical Signal Processing: Detection Theory*. Upper Saddle River, NJ, USA: Prentice Hall, 1998.

[29] S. M. Kay, *Fundamentals of Statistical Signal Processing: Estimation Theory*. Upper Saddle River, NJ, USA: Prentice-H, 1993.

[30] F. Kschischang, B. Frey, and H.-A. Loeliger, "Factor graphs and the sum-product algorithm," *IEEE Trans. Inf. Theory*, vol. 47, no. 2, pp. 498–519, Feb. 2001.

[31] D. Schuhmacher, B.-T. Vo, and B.-N. Vo, "A consistent metric for performance evaluation of multi-object filters," *IEEE Trans. Signal Process.*, vol. 56, no. 8, pp. 3447–3457, Aug. 2008.

[32] Y. Bar-Shalom, T. Kirubarajan, and X.-R. Li, *Estimation with Applications to Tracking and Navigation*. New York, NY, USA: Wiley, 2002.